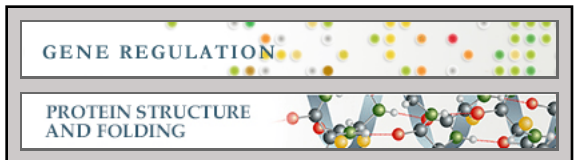


### Gene Regulation:

A Novel Protein-Protein Interaction in the RES (REtention and Splicing) Complex

Konstantinos Tripsianes, Anders Friberg, Charlotte Barrandon, Mark Brooks, Herman van Tilbeurgh, Bertrand Seraphin and Michael Sattler

J. Biol. Chem. published online August 26, 2014



Access the most updated version of this article at doi: 10.1074/jbc.M114.592311

Find articles, minireviews, Reflections and Classics on similar topics on the JBC Affinity Sites.

#### Alerts:

- When this article is cited
- · When a correction for this article is posted

Click here to choose from all of JBC's e-mail alerts

This article cites 0 references, 0 of which can be accessed free at http://www.jbc.org/content/early/2014/08/26/jbc.M114.592311.full.html#ref-list-1

### JBC Papers in Press. Published on August 26, 2014 as Manuscript M114.592311 The latest version is at http://www.jbc.org/cgi/doi/10.1074/jbc.M114.592311

Structure of RES Snu17p-Bud13p interaction

A Novel Protein-Protein Interaction in the RES (REtention and Splicing) Complex

### Konstantinos Tripsianes<sup>1\*</sup>, Anders Friberg<sup>2,3,#</sup>, Charlotte Barrandon<sup>4,§</sup>, Mark Brooks<sup>5,‡</sup>, Herman van Tilbeurgh<sup>5</sup>, Bertrand Seraphin<sup>4,6</sup>, and Michael Sattler<sup>2,3\*</sup>

- <sup>1</sup> Central European Institute of Technology (CEITEC), Masaryk University, Kamenice 5, 62500 Brno, Czech Republic
- <sup>2</sup> Institute of Structural Biology, Helmholtz Zentrum München, Ingolstädter Landstr. 1, 85764 Neuherberg, Germany
- <sup>3</sup> Center for Integrated Protein Science Munich and Chair of Biomolecular NMR, TU München, Lichtenbergstr. 4, 85747 Garching, Germany
- <sup>4</sup>Centre de Génétique Moléculaire, CNRS, Avenue de la Terrasse, 91198 Gif sur Yvette, France
- <sup>5</sup> Univ. Paris-Sud, Institut de Biochimie et de Biophysique Moléculaire et Cellulaire, UMR8619, F-91405 Orsav. France
- <sup>6</sup> Equipe Labellisée La Ligue, Institut de Génétique et de Biologie Moléculaire et Cellulaire (IGBMC), Centre National de Recherche Scientifique (CNRS) UMR 7104/Institut National de Santé et de Recherche Médicale (INSERM) U964/Université de Strasbourg, 67404 Illkirch, France
- \* Present address: Bayer HealthCare Pharmaceuticals, Lead Discovery, Müllerstr. 178, 13353 Berlin, Germany
- § Present address: Promega France, Parc d'Activités des Verrières, 24 Chemin des Verrières, 69260 Charbonnières, France
- <sup>‡</sup> Present address: Evotec (UK) Ltd, 114 Milton Park, Abingdon, OX14 4SA, UK

Running title: Structure of RES Snu17p-Bud13p interaction

\*To whom correspondence should be addressed: Konstantinos Tripsianes, Central European Institute of Technology, Masaryk University, Kamenice 5, 62500 Brno, Czech Republic, Tel: +420 549 49 6607. Fax: +420 549 49 2556. E-mail: kostas.tripsianes@ceitec.muni.cz or Michael Sattler. Institute of Structural Biology, Helmholtz Zentrum München, Ingolstädter Landstrasse 1, 85764 Neuherberg, Tel.: +49 89 3187-3800, Fax: +49 89 289-13869, E-Mail: sattler@helmholtz-muenchen.de

**Keywords:** Splicing, U2AF homology motif, RNA recognition motif, protein-protein interaction

**Background**: The heterotrimeric REtention and Splicing (RES) complex is conserved from yeast to man.

**Results**: Structural and biochemical analyses show an extended binding interface between the Snu17p RNA Recognition Motif (RRM) and Bud13p of the RES complex.

**Conclusions**: The Snu17p RRM-Bud13p interaction represents a novel RRM-protein interface.

**Significance**: The Snu17p-Bud13p complex may provide a platform for additional protein and RNA interactions in the RES complex.

#### **Abstract**

The REtention and Splicing (RES) complex is a conserved spliceosome-associated module that was shown to enhance splicing of a subset of transcripts and to promote the nuclear retention of unspliced pre-mRNAs in yeast. The heterotrimeric RES complex is organized around the Snu17p protein that binds to both the Bud13p and Pml1p subunits. Snu17p exhibits an RRM domain that resembles a U2AF homology motif (UHM) and Bud13p harbors a Trp residue reminiscent of an UHM-ligand motif (ULM). It has therefore been proposed that the interaction between Snu17p and Bud13p resembles canonical UHM-ULM complexes. Here, we have used biochemical and NMR structural analysis to characterize the structure of the yeast Snu17p-Bud13p complex. Unlike known UHMs that sequester the Trp residue of the ULM ligand in a hydrophobic pocket, Snu17p and Bud13p utilize a large interaction surface formed around the two helices of the Snu17p domain. In total eighteen residues of Bud13p ligand wrap around the Snu17p helical surface in an U-turn-like arrangement. The invariant Trp232 in Bud13p is located in the center of the turn, and contacts surface residues of Snu17p. The structural data are supported by mutational analysis and indicate that the Snu17p provides an extended binding surface with Bud13p that is notably distinct from canonical UHM-ULM interactions. Our data highlight structural diversity RNA recognition motif (RRM)-protein interactions, analogous to the one seen in for nucleic acid interactions.

#### Introduction

RNA splicing is one of the fundamental processes in constitutive and regulated gene expression in eukaryotes. During splicing, introns present in primary transcripts (pre-mRNAs) are removed and exons are ligated to produce translationally competent mRNAs. The reaction is mediated by the spliceosome, a highly dynamic machinery of five small nuclear ribonucleoprotein (snRNP) particles and a large number of non-snRNP interacting proteins (1). In the course of the splicing reaction snRNPs assemble stepwise and undergo substantial conformational rearrangements that allows processing of a wide variety of transcripts. In addition, non-snRNP proteins associate and exchange at different stages of the splicing process, allowing for further splicing regulation or coupling of splicing to other cellular processes (2).

A non-snRNP complex has been recently identified in Saccharomyces cerevisiae that enhances pre-mRNA splicing and prevents leakage of unspliced pre-mRNAs from the nucleus (3). The yeast pre-mRNA REtention and Splicing complex, called the RES complex, consists of the Snu17p, Bud13p and Pml1p proteins. Snu17p acts as a central platform, which independently binds Bud13p and Pml1p (4-6). The RES subunits and their human orthologs have been shown to associate transiently with the spliceosome prior to the first catalytic step that leads to intron excision (7.8). Yeast strains carrying deletions of Snu17p. Bud13p or Pml1p are viable but exhibit slow growth, a phenotype exacerbated at high temperatures. In vitro and in vivo splicing assays have demonstrated that RES complex enhances splicing, especially of those introns that contain poor consensus sequence at the 5' splice site (3,9), including alternatively spliced genes (10). Inactivation of RES subunits also induces leakage of pre-mRNAs from the nucleus to the cytoplasm, indicating that the RES complex has an important role in nuclear retention of unspliced transcripts (3). Finally, the RES complex was recently shown to facilitate the splicing of introns with short 5' splice site - branchpoint distances (11) and to interact genetically with the enzyme mediating trimethylation of the U snRNAs (12).

Of the three RES subunits, Snu17p contains an RNA recognition motif (RRM) domain (Figure 1). The RRM motif is the most abundant RNAbinding domain in higher vertebrates and found in many spliceosomal proteins. RRMs usually exhibit a compact fold comprised of four- or five-stranded β-sheet that represents the RNA binding surface and two  $\alpha$  helices packed against the  $\beta$ -sheet. Sequence conservation between various RRMs is low except three aromatic side-chains belonging to the two signature sequences RNP1 and RNP2, which are responsible for RNA binding (Figure 1a,c) (13,14). The UHM (U2AF homology motif) domain is a variant of the RRM domain and has been shown to mediate protein-protein interactions via the  $\alpha$ -helical face of the RRM fold (15). UHM domains often lack the aromatic residues in the RNP signature sequences and thus do not or only poorly bind to RNA. A Arg-X-Phe motif in UHM domain is involved in the recognition of a conserved tryptophan residue in the UHM ligand (ULMs). Structural studies motifs have demonstrated a common mode of ligand recognition by different UHM domains (15-19). The invariant Trp residue in the ULM (Figure 1b) inserts into a tight hydrophobic pocket formed by the two helices and the Arg-X-Phe motif of the UHM domain (Figure 1d), while positively charged residues preceding the conserved Trp in the ULM motif interact with negatively charged residues on the UHM domain.

Previous biochemical studies have indicated that the RRM domain of Snu17p is sufficient for binding Bud13p. Although some unconventional features of the Snu17p domain were noticed, such as the absence of the Arg-X-Phe motif (Figure 1a), it has been proposed that the Snu17p-Bud13p interaction follows the structural characteristics of UHM-ULM interactions (4,6,20). To better understand how the RES complex is organized to perform its biological functions we have determined the binary complex structure between Snu17p and Bud13p. Isothermal titration calorimetry (ITC) together with NMR binding experiments allowed the identification of the minimal length of the Bud13p ligand. The NMRderived solution structure shows that Snu17p and Bud13p do not interact through an UHM-ULM type of recognition. Rather, the interaction involves eighteen residues of Bud13p that contact

the helical surface of the Snu17p RRM domain. Notably, the invariant Trp of Bud13p is not buried in a hydrophobic cavity, distinct from canonical UHM-ULM interactions. The structural data are supported by mutational analysis of the interacting partners testing for their ability to form the RES complex when co-expressed in  $E.\ coli$  or to restore the growth phenotype of  $\Delta Snu17p$  or  $\Delta Bud13p$  strains.

### **Experimental procedures**

Cloning, protein expression and purification

Snu17p proteins (residues 1-113 or 25-113) and Bud13p proteins (residues 201-266 or 222-256) were cloned into a modified pET-24d vector using standard protocols. The fusion proteins expressed from these vectors comprise a His6-tag followed by a GST fusion domain and a tobacco etch virus (TEV) proteolytic cleavage site. Proteins were expressed in Escherichia coli BL21 (DE3) pLysS (Novagen) using kanamycin for selection. A 10mL Luria broth (LB) pre-culture was inoculated with a single colony from a transformation plate. The pre-culture was used to start larger 1L cultures, containing LB or M9 minimal medium for labeling with <sup>15</sup>N or <sup>15</sup>N/<sup>13</sup>C. Upon reaching optical density (OD) of 0.6 cultures were induced 0.5 mM IPTG (Isopropyl with β-D-1thiogalactopyranoside) for 4h at 37° C.

Recombinant proteins were purified by sonicating the harvested cell pellet in 25mL Lysis buffer (20 mM TRIS pH 7.5, 300 mM NaCl, 10 mM imidazole, 1 mM DTT and 0.02% NaN<sub>3</sub>), also including protease inhibitors, RNase, lysozyme 0.2% IGEPAL. After high-speed centrifugation (20000 rpm, 30 min) and filtering, each supernatant was applied to Ni-NTA Agarose resin (Qiagen). Several rounds of washing were performed, with: Lysis buffer including 0.2% IGEPAL, Lysis buffer, Lysis buffer with high salt concentration (1M NaCl), Lysis buffer with high imidazole concentration (30 mM imidazole). Finally, each protein was eluted by applying 10mL of a buffer containing 20 mM TRIS pH 7.5, 300 mM NaCl, 330 mM imidazole, 1 mM DTT and 0.02% NaN3. TEV protease was added to each sample and incubated overnight at 4°C. To remove the cleaved GST tag each sample was passed over a second Ni-NTA column. A second purification step included size exclusion chromatography (HiLoad, Superdex 75 16/60, GE Healthcare). In this step, proteins were buffer-exchanged into the NMR buffer (20 mM sodium phosphate pH 6.3, 25 mM NaCl and 2 mM fresh DTT or TCEP, 0.02% NaN<sub>3</sub>). Stoichiometric hybrid-labeled samples were prepared by mixing an excess of Bud13p with Snu17p and performing another step of size exclusion chromatography (HiLoad, Superdex 75 16/60, GE Healthcare).

Two shorter peptides of Bud13p (residues 221-242 or residues 225-238) were purchased from Peptide Specialty Laboratories (Heidelberg, Germany), and extensively dialyzed before binding experiments.

An operon system encoding His<sub>6</sub>-Snu17p, Bud13p and Pml1p was described earlier (4). Snu17p and Bud13p variants were introduced into this vector by standard mutagenesis and cloning procedures. Protein expression, complex mini-purifications and denaturing gel analyses of complex composition were performed as previously described (4).

#### NMR spectroscopy and structure calculation

NMR spectra were recorded at 298 K on an AVIII800 Bruker NMR spectrometer equipped with a cryogenic triple resonance gradient probe. Spectra were processed using NMRPipe (21). Protein backbone and side chain assignments were from standard triple experiments (22). NOE distance restraints were obtained from <sup>15</sup>N- and <sup>13</sup>C-edited 3D NOESY spectra (mixing time 70 ms) where only Snu17p or Bud13p protein was labeled. Intermolecular NOE restraints were derived from 3D <sup>15</sup>N. <sup>13</sup>C-filtered. <sup>13</sup>C-edited NOESY spectra (mixing time 70 ms) (22,23). Stereospecific assignments of pro-chiral methyl groups of valine and leucine were obtained using 10% <sup>13</sup>C-labeled protein samples (24).

Structure calculations with torsion angle dynamics were performed by using the program CYANA 3.0 (25). For every assigned peak, the distances between the protons (for a range between 2.4 and 6 Å) were calibrated using CYANA's calibration algorithm. The set of NOE distance restraints together with  $\phi$  and  $\psi$  backbone dihedral angle restraints derived from TALOS+ (26) based on the chemical shifts were used for water refinement (27) using CNS (28). The structure was validated

by using iCing (http://nmr.cmbi. ru.nl/icing/). Molecular images were generated with PyMol (Schrödinger).

#### Isothermal Titration Calorimetry

Calorimetric measurements were performed with a VP-ITC (MicroCal Inc.) instrument at 25° C using samples in NMR buffer. The concentration of Snu17p (residues 1-113) in the cell (1440  $\mu L$ ) varied between 30-70  $\mu M$ , while the syringe (300  $\mu L$ ) contained Bud13p ligands at concentrations ranging from 0.6 to 1.1 mM. Normally 50 injections were done over a period of 3-4 hours. Bud13p ligands were also injected into buffer and the heat of dilution control was subtracted from the titration. Data fitting was done in Origin v7 using one- or two-step binding models supplied by the manufacturer. The dissociation constant values are given with the fitting error.

#### In vivo analyses

The wild type SNU17 and BUD13 genes were cloned in the pRS425 plasmid backbone. The TAP tag coding sequence (29) was introduced to produce C-terminal fusions, allowing the monitoring of protein expression levels. Snu17p and Bud13p variants were introduced into the resulting vectors by standard mutagenesis and cloning procedures. These plasmids were transformed respectively into  $\Delta snu17$  or  $\Delta bud13$ strains (3,4). Transformants were selected and complementation was assayed by spotting serial dilutions of the strain on selective plates and indicated temperatures. incubating at the Expression of the wild type and mutant proteins was monitored by extracting total proteins and monitoring the levels of the TAP-tagged fusions by western blotting.

#### **Results**

#### RES complex assembly and function

Previous biochemical analyses have shown that Snu17p binds Bud13p directly (4,6). Based on a mutational analysis of the invariant Bud13p Trp232 residue (6), the interaction of Bud13p with the Snu17p RRM has been proposed to resemble a typical UHM-ULM interaction. Another study, however, showed that the W232A mutation did not abolish its interaction with Snu17p (4), in contrast to what has been reported for UHM-ULM

interactions so far (18). Moreover, it had been noticed that Snu17p lacks the UHM-characteristic Arg-X-Phe motif and also contains the RRM-typical consensus sequence motifs (RNP1 Phe74, Tyr76 and RNP2 Tyr34) that mediate RNA interactions in canonical RRM domains (**Figure 1a,c**).

To characterize the Snu17p-Bud13p interaction in vivo we performed mutational analysis in S. cerevisiae. We first tested the impact of mutations on complex formation in vitro by co-expressing His-Snu17p, Bud13p and Pml1p encoded by an operon in E. coli and assessing complex assembly by purification on Ni-NTA (4). A double or triple mutant around the conserved Trp residue (R231D+W232A or R231D+W232A+D233N) of Bud13p abolished Bud13p incorporation in the RES complex (Figure 2a). To assay the in vivo function, a yeast strain lacking the Bud13p gene (ΔBud13) was transformed with a vector carrying either the wild type Bud13p tagged with the TAP tag, or its double or triple mutant derivatives. Cells carrying the vector without insert were used as a negative control. At 30°C, the growth of both mutants was only mildly affected (slightly smaller colony sizes than wild type cells, Figure 2b). Consistent with previous observations deletion of bud13 resulted in a strong phenotype at 37 °C (3). In this condition, both mutants were barely different from cells transformed with the vector indicating that they were not functional. Transformation of the same Bud13p mutants in a wild type strain did not result in slow growth demonstrating that they were not functional rather than acting as dominant negatives. Moreover, growth deficiency was not due to a decreased expression of the mutant proteins (detected by western blot analyses of the TAP tag) (Figure 2c) excluding that the mutations acted simply by destabilizing the proteins. These data indicate that Trp232 of Bud13p indeed is important for the interaction with Snu17p but that flanking residues also contribute to the binding.

Snu17p mutants were designed based on sequence homology with UHM domains that utilize a hydrophobic pocket between the two helices of the UHM domain to accommodate the invariant Trp of the ULM ligand. We targeted the Snu17p residues corresponding to the Arg-X-Phe motif (95-FKI-97). A triple mutant (F95A+K96D+I97A)

did not disrupt RES complex formation as assayed by co-expression of the proteins in  $E.\ coli$  followed by Ni-NTA purification (**Figure 2a**). We also tested the ability of this mutant to rescue the growth phenotype of  $\Delta Snu17$  yeast cells. The mutant grew well at all temperatures tested (**Figure 2d**) both in the mutant and wild type strain backgrounds. Western blotting confirmed that the mutant was well expressed (**Figure 2e**). These results suggest that Snu17p may use a different interaction surface than canonical UHM proteins to bind the Bud13p ligand.

Biophysical analysis of Snu17p-Bud13p complex

To characterize the unexpected molecular features of the Snu17p-Bud13p interaction we proceeded with a biophysical and structural characterization of the binary complex (Figure 3). We first used a construct comprising the Snu17p RRM and an Nterminal unstructured (see below) extension (Snu17p, residues 1-113) as this domain was shown to be sufficient for the interaction with Bud13p (4,6). We tested binding to a series of Bud13p fragments to identify the minimum binding region in Bud13p (Figure 3a,b). NMR titrations confirmed binding to a Bud13p peptide encompassing residues 201-266 as has been shown previously (20). Addition of this peptide to recombinant <sup>15</sup>N-labeled Snu17p induced extensive chemical shift perturbations (CSPs) in <sup>1</sup>H, <sup>15</sup>N correlation spectra but also led to precipitation of the sample. Similar CSPs were observed with a shorter Bud13p peptide (residues 222-256) but proteins remained in solution (Figure 3b). An even shorter peptide (residues 221-242) affected the same Snu17p residues but to a lesser extent compared to the longer ones. Finally, a very short Bud13p peptide (residues 225-238) hardly induced any NMR spectral changes for Snu17p, even though this peptide has the typical length of ULM ligands and harbors the invariant Trp (Figure 3b). Thus, the NMR data indicate that recognition of a ULM-like motif with its central Trp residue is not sufficient for Bud13pcomplex formation. This further Snu17p demonstrates a different recognition mode involving additional residues present in the longer Bud13p peptides.

The Snu17p-Bud13p interaction was further characterized by isothermal titration calorimetry

(ITC) to quantitate the binding affinity and characterize the thermodynamic features of the interaction. The binding isotherms of the two longer peptides show low nanomolar binding affinity. The calorimetric analysis also suggests a second interaction at large excess of Bud13, however, with a lower affinity with binding constants separated by two orders of magnitude (Figure 3a), potentially reflecting an additional non-specific interaction. In any case, the ITC data corroborate the NMR findings that the additional residues present in the very long Bud13p peptide do not contribute to Snu17p binding when compared to the Bud13p 222-256 peptide. The low nanomolar binding affinities are in very good agreement with the thermodynamic binding parameters of the full-length Snu17p-Bud13p complex (6). The ITC titration of Snu17p with the shorter Bud13p peptide (residues 221-242) could be fitted to a single binding site with a dissociation constant 50 times weaker compared to the longer ligands (Figure 3a). The lower affinity is in accordance with quantitative information obtained from NMR chemical shift titration analysis for the Bud13p ligands (data not shown). For the shortest Bud13p peptide, the signal to noise ratio of the ITC signal was too small to make a precise determination of its binding constant, indicating that it binds very weakly consistent with the NMR titrations (Figure 3a,b). Based on NMR and ITC data we conclude that residues 222-256 of Bud13p encompass the minimum interacting region with Snu17p.

Next, we assigned the backbone chemical shifts of Snu17p (residues 1-113) when free and in a stoichiometric complex with unlabeled Bud13p (residues 222-256). Chemical shift analysis shows that Snu17p contains the expected secondary structure elements of an RRM domain in both free and bound forms (Figure 3c), i.e. the secondary structure is preserved upon Bud13p binding. The first 25 residues of Snu17p do not exhibit any secondary structure and {1H}-15N heteronuclear NOE data show that the N-terminus preceding the RRM domain is highly flexible (Figure 3c). The residues showing large chemical shift changes, induced by Bud13p binding, map on the two helices plus adjacent loop regions of the Snu17p RRM fold indicating a large interaction surface (Figure 3c). These CSPs are distinct from what

would be expected for a canonical UHM-ULM interaction, demonstrating that Snu17p and Bud13p use a different binding interface. Virtually identical NMR CSPs induced by Bud13p binding to a shorter Snu17p protein (residues 25-113) demonstrating that the flexible Snu17p N-terminus does not participate in the interaction (data not shown).

The Snu17p-Bud13p interaction was characterized by monitoring NMR signals of <sup>15</sup>Nlabeled Bud13p (residues 222-256) in complex with unlabeled Snu17p. Binding to Snu17p induces extensive chemical shift changes in Bud13p spectra (Figure 4a). Secondary chemical shift analysis indicates the presence of an  $\alpha$ -helical segment at the C-terminus of the bound Bud13p peptide (Figure 4b). Steady state {<sup>1</sup>H}-<sup>15</sup>N heteronuclear NOE data show that a large portion of the peptide is rigid in the complex suggesting that the region comprising Bud13p residues 222-246 contributes to the Snu17p binding interface directly or become less flexible due to complex formation (Figure 4b). Interestingly, the Cterminal helical region remains partially flexible.

#### Structure of the Snu17p-Bud13p complex

We then determined the solution structure of the Snu17p-Bud13p complex (comprising Snu17p residues 25–113 and Bud13p residues 222-256) by heteronuclear triple-resonance NMR spectroscopy using subunit-selectively isotope-labeled samples. The two proteins were prepared separately and copurified by size exclusion chromatography after mixing an excess of Bud13p with Snu17p. In this way we were able to selectively label each of the proteins in the complex and determine 129 intermolecular distance restraints, derived from <sup>13</sup>C- and <sup>15</sup>N-edited NOESY HSOC spectra as well as <sup>13</sup>C/<sup>15</sup>N-filtered and <sup>13</sup>C-edited NOESY-HSOC spectra (Figure 5). The structure of the complex is well-defined and based on 2607 experimental distance restraints, including (Figure 6). A summary of the structural and restraint statistics is given in Table 1. The ensemble of the 20 lowest energy structures obtained after water refinement is shown in Figure 6a.

In the complex Snu17p adopts an RRM fold with two  $\alpha$ -helices packing on one surface of an antiparallel  $\beta$ -sheet (**Figure 6b**). The Snu17p structure superimposes very well with UHM

family members (RMSD 1.5-1.8 Å for 72  $C_{\alpha}$  atoms against the proteins listed in **Figure 1a**). Noteworthy, although most UHM family members lack the conserved aromatic residues in RNP1 and RNP2 that mediate RNA binding in canonical RRMs, Snu17p has retained both RNPs. However, the structure shows that Tyr76 (RNP1) is not solvent exposed but rather stacks parallel with another tyrosine (Tyr109) located at the C-terminal extension of the RRM fold (**Figure 6c**). The partial solvent protection of the RNP1 motif may imply potential regulation of RNA binding by Snu17p in the RES complex.

Bud13p binds to the helical surface of the RRM domain of Snu17p, consistent with the chemical shift mapping data (Figure 6b). Although Bud13p contains the invariant Trp residue of ULMs, the interaction is distinct from the canonical UHM-ULM recognition. Bud13p assumes an extended conformation and forms an arch around the Snu17p RRM above the two Snu17p helices. Two glycine residues flanking the invariant Trp that are not present in other ULMs change the backbone direction of the Bud13p on the surface of Snu17p. Eighteen amino acids of Bud13p interact with Snu17p forming a U-turn that crosses the helical interface of Snu17p (Figure 6b). The invariant Trp is located in the middle of the turn and is recognized together with the flanking interacting residues of Bud13p on the surface of Snu17p (**Figure 6b**). The C-terminal helix of the Bud13p ligand does not contribute to the binding interface and its orientation is not defined by experimental data. This suggests that it is flexible in solution. consistent with reduced heteronuclear {1H}-15N NOE values (Figure 4b). The Snu17p/Bud13p binding surface area covers ~800 Å<sup>2</sup>, and is thus significantly larger compared to any UHM-ULM interaction described so far (Figure 6d).

The binding interface between Snu17p and Bud13p is mainly stabilized by hydrophobic interactions. The extensive bipartite hydrophobic interface includes the whole stretch of residues from Asn222 to Asn239 of Bud13p and the dorsal helical face of Snu17p RRM domain. The apolar contacts are supported by electrostatic interactions involving mainly backbone amide groups of Bud13p (**Figure 6d**). The entire backbone of the Bud13p stretch is involved in intermolecular contacts but certain amino acids engage their side

chains as well, thus contributing more to the interaction. Three regions of higher significance can be discerned based on intermolecular NOE data and the relative contribution to the total interaction surface (Figure 7a). The first spot is at the N-terminus of Bud13p where it enters the interaction surface and passes above helix α2 of Snu17p. Phe224 and Ile226 of Bud13p exhibit mainly hydrophobic contacts with the helical interface lined by Snu17p Arg83, Ser84, Ile86, and Leu87 (**Figure 7b**). The second binding hotspot is at the U-turn of Bud13p. Bud13p residues from Pro228 to Val235 encircle the indole ring of the invariant Bud13p Trp232. The conformation of the Bud13p peptide is supported by many intramolecular NOEs between Bud13p Trp232 and Pro228 on one side and Val235 on the other side. The presence of Gly229 following Pro228 and Gly234 preceding Val235 provide the conformational flexibility required for reversing the backbone course of Bud13p. In the U-turn configuration Pro228, Arg231, Trp232, and Val235 of Bud13p form a continuous surface that interacts with Snu17p helix α1 (residues Leu48, Thr49, Ser52, and Glu53), as well as Snu17p Val56 in the linker following helix  $\alpha 1$  (**Figure 7b**). The third interface involves Snu17p Val50, Phe95 and Asn91, which contact Bud13p Arg237, Ser238 and Asn239, respectively at the crevice between the two a-helices of the Snu17p RRM (Figure 7b). This interface is further stabilized by hydrogen bonds between the Bud13p backbone and Snu17p sidechains. At this point Bud13p ligand exits the binding interface with Snu17p and assumes a helical conformation.

#### **Discussion**

The solution structure of Snu17p-Bud13p reveals a novel binding mode that has not been observed in other RRM/UHM peptide complexes. structural findings are consistent with our initial mutagenesis analysis, which was guided by the recognition features described for the UHM family. We found that a double or triple mutant around the invariant Trp residue of Bud13p (R231D+W232A or R231D+W232A+D233N) disrupted Snu17p binding in vitro, and impacted on normal cell growth of transformants while the single W232A substitution did not prevent complex formation (4) - in contrast to canonical UHM-ULM interactions (18,30). On the other hand, a triple mutant of

Snu17p residues that correspond to the UHM Arg-X-Phe motif (F95A+K96D+I97A) had no effect in the formation of RES complex and restored a growth phenotype similar to wild type. These findings indicated an unexpected architecture of recognition that is distinct from the established UHM-ULM mode.

Several structures have revealed the main features that determine UHM-ULM interactions (16-19,30,31). UHM domains typically lack one or more aromatic residues in their RNP sequences, they have an acidic helix al, and contain an Arg-X-Phe motif following the second helix  $\alpha 2$ . The Arg-X-Phe motif recognize ULM sequences that contain an invariant Trp residue that is usually preceded by basic residues. The critical Trp is inserted into a hydrophobic cleft formed between the two helices of the UHM fold with the ULM peptide oriented perpendicular to the two helices (Figure 8a). In general, UHM domains do not interact with RNA as often the RNA-binding βsheet surface on the opposite side of the RRM fold is occluded by a C-terminal helix.

An interesting variation of the UHM-ULM theme is the interaction between the PTB protein and its corepressor Raver1 (32). The consensus signature motif of Raver1 ligands do not harbor the Trp residue but instead a pair of Leu residues. The PTB structures in complex with two peptide motifs from Raver1 (33) show that the Leu residues substitute for the Trp recognition seen in UHM-ULM binding and interact with a shallow groove formed at the same location on PTB RRM2 domain (**Figure 8b**). Interestingly, it has been reported that the PTB RRM2 domain can bind simultaneously Raver1 and RNA, a distinctive feature that has not been described for other UHM domains.

The most notable exception of RRM binding to Trp containing ligands has been reported for the cellular mRNA export factor ALYREF (34). Two structures have been determined of ALYREF RRM domain in complex with viral peptides, both of them different from the UHM-ULM mode (**Figure 8c**). The ICP27 peptide binds ALYREF RRM in an extended conformation along the groove formed by the helices (34). The Trp residue is located at the upper edge of the first ALYREF helix and contributes to the

interaction surface. The ORF57 peptide on the other hand adopts a helical conformation running almost perpendicular to the helices of ALYREF (35). The Trp residue is positioned at one end of the helix and makes hydrophobic contacts with ALYREF along with other residues of the helical peptide. Mutational analysis indicates that in ORF57 the Trp residue is important for ALYREF recognition, whereas in ICP27 is not as crucial as has been demonstrated for true UHM-ULM pairs.

The structure of Snu17p-Bud13p complex presented here displays yet another distinct binding topology that has not been described before, further adding to the diversity of RRMligand interactions. A large portion of the Bud13p ligand is engaged in contacts around the helical surface of Snu17p. The Trp residue is located in the middle of a U-turn configuration that collectively contacts the first helix of Snu17p (Figure 8d). Preceding and following residues to the U-turn are perpendicular to the second helix of Snu17p and contribute to binding. The importance of these residues to the interaction, which are rather distant to the invariant Trp, has been confirmed by in vitro binding studies designed to identify the minimal interacting region on Bud13p. Notably, key residues in Bud13p involved in Snu17p binding are conserved (data not shown) in other orthologs including the human homolog of Bud13p, suggesting that the novel mode of RRMpeptide interaction is conserved.

The yeast RES complex facilitates the splicing of some introns and participates in the retention of unspliced pre-mRNAs in the nucleus. The absence of a functional RES complex in yeast results in slow growth, particularly at high temperature, due to reduced splicing (3). Our data show that preventing the association of Bud13p with Snu17p impairs cell growth without affecting protein expression levels. This demonstrates individual proteins when simultaneously present are unable to perform the RES activity and thus that assembly of the RES complex is essential for function. It is conceivable that to perform its task the RES complex recognizes specific RNA sequences through its Snu17p subunit. The Snu17p-Bud13p structure shows that Bud13p binding does not interfere with the RNP sequences of Snu17p. Snu17p could thus be involved in RNA recognition as shown for canonical RRM domains

(13,14). However, in Snu17p the first RNP motif is partially occluded from the solvent by the C-terminal tail of the RRM fold. We envisage that Pml1p may regulate RNA binding of Snu17p in the functional ternary RES complex. The binding of Pml1p, which requires the Snu17p C-terminal portion in addition to the RRM fold, could induce

structural rearrangements that might completely expose the RNP motifs of Snu17p. Future studies with the ternary RES complex and RNA should shed light to this hypothesis and increase our understanding for RES function in RNA splicing and nuclear retention of pre-messenger transcripts.

#### References

- 1. Jurica, M. S., and Moore, M. J. (2003) Pre-mRNA splicing: awash in a sea of proteins. *Molecular cell* 12, 5-14
- Wahl, M. C., Will, C. L., and Luhrmann, R. (2009) The spliceosome: design principles of a dynamic RNP machine. Cell 136, 701-718
- Dziembowski, A., Ventura, A. P., Rutz, B., Caspary, F., Faux, C., Halgand, F., Laprevote, O., and Seraphin, B. (2004) Proteomic analysis identifies a new complex required for nuclear pre-mRNA retention and splicing. *The EMBO journal* 23, 4847-4856
- 4. Brooks, M. A., Dziembowski, A., Quevillon-Cheruel, S., Henriot, V., Faux, C., van Tilbeurgh, H., and Seraphin, B. (2009) Structure of the yeast Pml1 splicing factor and its integration into the RES complex. *Nucleic acids research* 37, 129-143
- 5. Trowitzsch, S., Weber, G., Luhrmann, R., and Wahl, M. C. (2009) Crystal structure of the Pml1p subunit of the yeast precursor mRNA retention and splicing complex. *Journal of molecular biology* 385, 531-541
- 6. Trowitzsch, S., Weber, G., Luhrmann, R., and Wahl, M. C. (2008) An unusual RNA recognition motif acts as a scaffold for multiple proteins in the pre-mRNA retention and splicing complex. *The Journal of biological chemistry* 283, 32317-32327
- Deckert, J., Hartmuth, K., Boehringer, D., Behzadnia, N., Will, C. L., Kastner, B., Stark, H., Urlaub, H., and Luhrmann, R. (2006) Protein composition and electron microscopy structure of affinity-purified human spliceosomal B complexes isolated under physiological conditions. *Molecular and cellular biology* 26, 5528-5543
- 8. Bessonov, S., Anokhina, M., Will, C. L., Urlaub, H., and Luhrmann, R. (2008) Isolation of an active step I spliceosome and composition of its RNP core. *Nature* 452, 846-850
- 9. Dreumont, N., and Seraphin, B. (2013) Rapid screening of yeast mutants with reporters identifies new splicing phenotypes. *The FEBS journal* 280, 2712-2726
- 10. Scherrer, F. W., Jr., and Spingola, M. (2006) A subset of Mer1p-dependent introns requires Bud13p for splicing activation and nuclear retention. *Rna* 12, 1361-1372
- 11. Zhou, Y., Chen, C., and Johansson, M. J. (2013) The pre-mRNA retention and splicing complex controls tRNA maturation by promoting TAN1 expression. *Nucleic acids research* 41, 5669-5678
- 12. Hausmann, S., Zheng, S., Costanzo, M., Brost, R. L., Garcin, D., Boone, C., Shuman, S., and Schwer, B. (2008) Genetic and biochemical analysis of yeast and human cap trimethylguanosine synthase: functional overlap of 2,2,7-trimethylguanosine caps, small nuclear ribonucleoprotein components, pre-mRNA splicing factors, and RNA decay pathways. *The Journal of biological chemistry* 283, 31706-31718
- 13. Daubner, G. M., Clery, A., and Allain, F. H. (2013) RRM-RNA recognition: NMR or crystallography...and new findings. *Current opinion in structural biology* 23, 100-108
- 14. Maris, C., Dominguez, C., and Allain, F. H. (2005) The RNA recognition motif, a plastic RNA-binding platform to regulate post-transcriptional gene expression. *The FEBS journal* 272, 2118-2131
- 15. Kielkopf, C. L., Lucke, S., and Green, M. R. (2004) U2AF homology motifs: protein recognition in the RRM world. *Genes & development* 18, 1513-1526

- Corsini, L., Bonnal, S., Basquin, J., Hothorn, M., Scheffzek, K., Valcarcel, J., and Sattler, M. (2007) U2AF-homology motif interactions are required for alternative splicing regulation by SPF45. *Nature structural & molecular biology* 14, 620-629
- 17. Corsini, L., Hothorn, M., Stier, G., Rybin, V., Scheffzek, K., Gibson, T. J., and Sattler, M. (2009) Dimerization and protein binding specificity of the U2AF homology motif of the splicing factor Puf60. *The Journal of biological chemistry* 284, 630-639
- 18. Selenko, P., Gregorovic, G., Sprangers, R., Stier, G., Rhani, Z., Kramer, A., and Sattler, M. (2003) Structural basis for the molecular recognition between human splicing factors U2AF65 and SF1/mBBP. *Molecular cell* 11, 965-976
- 19. Loerch, S., Maucuer, A., Manceau, V., Green, M. R., and Kielkopf, C. L. (2014) Cancer-Relevant Splicing Factor CAPERalpha Engages the Essential Splicing Factor SF3b155 in a Specific Ternary Complex. *The Journal of biological chemistry*
- 20. Collinet, B., Friberg, A., Brooks, M. A., van den Elzen, T., Henriot, V., Dziembowski, A., Graille, M., Durand, D., Leulliot, N., Saint Andre, C., Lazar, N., Sattler, M., Seraphin, B., and van Tilbeurgh, H. (2011) Strategies for the structural analysis of multi-protein complexes: lessons from the 3D-Repertoire project. *J Struct Biol* 175, 147-158
- 21. Delaglio, F., Grzesiek, S., Vuister, G. W., Zhu, G., Pfeifer, J., and Bax, A. (1995) NMRPipe: a multidimensional spectral processing system based on UNIX pipes. *J Biomol NMR* 6, 277-293
- 22. Sattler, M., Schleucher, J. r., and Griesinger, C. (1999) Heteronuclear multidimensional NMR experiments for the structure determination of proteins in solution employing pulsed field gradients. *Progress in Nuclear Magnetic Resonance Spectroscopy* 34, 93-158
- 23. Breeze, A. L. (2000) Isotope-filtered NMR methods for the study of biomolecular structure and interactions. *Progress in Nuclear Magnetic Resonance Spectroscopy* 36, 323-372
- 24. Neri, D., Szyperski, T., Otting, G., Senn, H., and Wuthrich, K. (1989) Stereospecific nuclear magnetic resonance assignments of the methyl groups of valine and leucine in the DNA-binding domain of the 434 repressor by biosynthetically directed fractional <sup>13</sup>C labeling. *Biochemistry* 28, 7510-7516
- 25. Guntert, P. (2009) Automated structure determination from NMR spectra. Eur Biophys J 38, 129-143
- 26. Shen, Y., Delaglio, F., Cornilescu, G., and Bax, A. (2009) TALOS+: a hybrid method for predicting protein backbone torsion angles from NMR chemical shifts. *J Biomol NMR* 44, 213-223
- 27. Linge, J. P., Williams, M. A., Spronk, C. A., Bonvin, A. M., and Nilges, M. (2003) Refinement of protein structures in explicit solvent. *Proteins* 50, 496-506
- 28. Brunger, A. T., Adams, P. D., Clore, G. M., DeLano, W. L., Gros, P., Grosse-Kunstleve, R. W., Jiang, J. S., Kuszewski, J., Nilges, M., Pannu, N. S., Read, R. J., Rice, L. M., Simonson, T., and Warren, G. L. (1998) Crystallography & NMR system: A new software suite for macromolecular structure determination. *Acta Crystallographica Section D: Biological Crystallography* 54, 905-921
- Rigaut, G., Shevchenko, A., Rutz, B., Wilm, M., Mann, M., and Seraphin, B. (1999) A generic protein purification method for protein complex characterization and proteome exploration. *Nat Biotechnol* 17, 1030-1032
- 30. Kielkopf, C. L., Rodionova, N. A., Green, M. R., and Burley, S. K. (2001) A novel peptide recognition mode revealed by the X-ray structure of a core U2AF35/U2AF65 heterodimer. *Cell* 106, 595-605
- 31. Elantak, L., Wagner, S., Herrmannova, A., Karaskova, M., Rutkai, E., Lukavsky, P. J., and Valasek, L. (2010) The indispensable N-terminal half of eIF3j/HCR1 cooperates with its structurally conserved binding partner eIF3b/PRT1-RRM and with eIF1A in stringent AUG selection. *Journal of molecular biology* 396, 1097-1116
- 32. Rideau, A. P., Gooding, C., Simpson, P. J., Monie, T. P., Lorenz, M., Huttelmaier, S., Singer, R. H., Matthews, S., Curry, S., and Smith, C. W. (2006) A peptide motif in Raver1 mediates splicing repression by interaction with the PTB RRM2 domain. *Nature structural & molecular biology* 13, 839-848

- 33. Joshi, A., Coelho, M. B., Kotik-Kogan, O., Simpson, P. J., Matthews, S. J., Smith, C. W., and Curry, S. (2011) Crystallographic analysis of polypyrimidine tract-binding protein-Raver1 interactions involved in regulation of alternative splicing. *Structure* 19, 1816-1825
- 34. Tunnicliffe, R. B., Hautbergue, G. M., Kalra, P., Jackson, B. R., Whitehouse, A., Wilson, S. A., and Golovanov, A. P. (2011) Structural basis for the recognition of cellular mRNA export factor REF by herpes viral proteins HSV-1 ICP27 and HVS ORF57. *PLoS pathogens* 7, e1001244
- 35. Tunnicliffe, R. B., Hautbergue, G. M., Wilson, S. A., Kalra, P., and Golovanov, A. P. (2014) Competitive and cooperative interactions mediate RNA transfer from herpesvirus saimiri ORF57 to the mammalian export adaptor ALYREF. *PLoS pathogens* 10, e1003907

#### Acknowledgements

We thank the members of the Sattler and Séraphin groups for discussion and advice. We acknowledge NMR measurement time at the Bavarian NMR Centre, Garching, Germany. A.F. is grateful for support by the Elitenetzwerk Bayern. This work was supported by the European Social Fund and the state budget of the Czech Republic (CZ.1.07/2.3.00/20.0042) [K.T.], the Centre National pour la Recherche Scientifique [B.S], the grant ANR-10-LABX-0030-INRT managed under the programme Investissements d'Avenir ANR-10-IDEX-0002-02 to [B.S.], the European Union Sixth Framework program "3D-Repertoire" [LSHG-CT-2005-512028 to B.S. and M.S.] and EURASNET [LSHG-CT-2005- 518238 to B.S.], the Ligue Contre le Cancer (Equipe Labellisée 2014) [to B.S.], the CERBM-IGBMC [to B.S.], the Deutsche Forschungsgemeinschaft [grant SFB1035 to M.S.].

#### Figure legends

**Figure 1.** Sequence and structural features of RRM and UHM domains. (a) Structure-based sequence alignment of UHM/RRM domains. Secondary elements are indicated on top and residue numbers of Snu17p are given at the bottom. Residues in the RNP motifs of Snu17p and the Arg-X-Phe motifs of UHM domains are colored cyan and red, respectively. Conserved residues in the motifs are highlighted by black boxes. (b) Sequence alignment of ULM peptide sequences known to bind UHM domains with the Bud13p ligand (residue numbers of Bud13p indicated at the bottom). The invariant tryptophan of ULM ligands and the two glycine residues that are unique to Bud13p are colored orange and magenta, respectively. Residues that form the binding interface between Snu17p and Bud13p are highlighted with limegreen background in (a) and (b), respectively. (c,d) Representative structures of a canonical RRM domain (PDB: 2G4B) in complex with RNA (c) and a representative UHM domain (PDB: 2PEH) bound to a ULM peptide (d). RNP motifs and the UHM-specific RXF sequence are annotated in β strands.

**Figure 2.** Mutational analyses of the Bud13p-Snu17p interaction. (a) Interactions between Snu17p, Bud13p and Pml1p were assayed by one-step Ni-NTA purification of wild type or mutant proteins coexpressed in *E. coli*. Supernatant (S) and (P) fractions from bacterial lysates as well as flow-through (F) and elution (E1, E2 and E3) fractions from the Ni-NTA purifications are shown after Coomassie staining of the gels. M indicates the molecular weight marker with size indicated on the left in kDa. Note that the Pml1p is less well stained than Snu17p and Bud13p. (b) Complementation of a Δbud13 strains with an empty vector, or plasmids expressing wild type or mutant Bud13p was monitored through the growth of serial dilutions of transformants on selective plates at the indicated temperatures. (c) Western blot showing the level of wild type and mutant Bud13p is detected through the fused TAP tag. (d) Complementation of a Δsnu17 strain was performed as for Bud13p in (b). (e) The levels of wild type and mutants Snu17p was monitored by detection of the TAP tag by western blotting.

**Figure 3.** ITC and NMR analysis of Snu17p binding to Bud13p (a) Four different Bud13p peptides containing the invariant Trp residue were tested by ITC titrations for Snu17p binding. Binding curves for a 66-mer, a 35-mer used in the accompanying structural studies, a 22-mer, and a 14-mer Bud13p peptide,

are depicted from left to right. Dissociation constants obtained by fitting the isotherms after subtracting the heat of dilution are listed. (b) Overlay of  $^1H$ ,  $^{15}N$  HSQC spectra of free Snu17p (residues 1-113, black) and after titration with the shortest Bud13p ligand (residues 225-238, orange) or with the optimal Bud13p peptide (residues 222-256, green). (c) Secondary  $^{13}C$  chemical shifts  $\Delta\delta(^{13}C^{\alpha})-\Delta\delta(^{13}C^{\beta})$  for Snu17p free and bound to Bud13p 222-256,  $\{^1H\}^{-15}N$  heteronuclear NOE of the Snu17p-Bud13p complex, and chemical shift perturbations of Snu17p amide signals (recorded on a sample of  $^{15}N$ -labeled Snu17 residues 25-113) upon binding to Bud13p 222-256 are plotted versus the amino acid sequence of Snu17p. Secondary structure elements of Snu17p are indicated on top.

**Figure 4.** NMR analysis Bud13p ligand (residues 222-256) binding to Snu17p. (a) Overlay of the  $^{1}$ H,  $^{15}$ N HSQC spectra of the Bud13p ligand free and when bound to Snu17p (b) Secondary  $^{13}$ C chemical shifts  $\Delta\delta(^{13}C^{\alpha}-^{13}C^{\beta})$  and  $^{1}$ H $^{15}$ N heteronuclear NOE data for the Bud13p ligand when bound to Snu17p. The last 5 residues of Bud13p have negative NOE values and are not shown. The short helix in the C-terminal region of the peptide is indicated on top.

**Figure 5.**  $^{1}$ H ( $\omega_{3}$ ),  $^{1}$ H ( $\omega_{1}$ ) planes from  $^{13}$ C/ $^{15}$ N-filtered,  $^{13}$ C-edited NOESY-HSQC spectra in the binary complex composed of doubly labeled Snu17p and unlabeled Bud13p. The  $^{13}$ C chemical shifts (ppm) of the selected  $\omega_{2}$  planes are indicated on top. The experiment selects NOE cross peaks between protons bound to  $^{12}$ C or  $^{14}$ N in Bud13p and protons bound to  $^{13}$ C in Snu17p, providing exclusively intermolecular restraints. For each cross peak the upper and lower atom name refers to Snu17p and Bud13p assignments, respectively.

**Figure 6.** Structure of the Snu17p-Bud13p complex. (a) Overlay of the 20 lowest energy structures of Snu17p (blue) in complex with Bud13p (yellow). The N and C terminus of each protein is annotated. (b) Cartoon representation of the Snu17p-Bud113p complex with amide chemical shift perturbations (CSP) induced by Bud13p binding mapped onto the structure with a color gradient white to blue with increasing CSP. The invariant Trp residue of Bud13p is shown as stick representation. (c) The RNP signature motifs of Snu17p (Tyr34, Phe74, Tyr76) are conserved but not entirely exposed to the solvent. (d) Electrostatic surface of Snu17p with negative and positive charge colored red and blue, respectively.

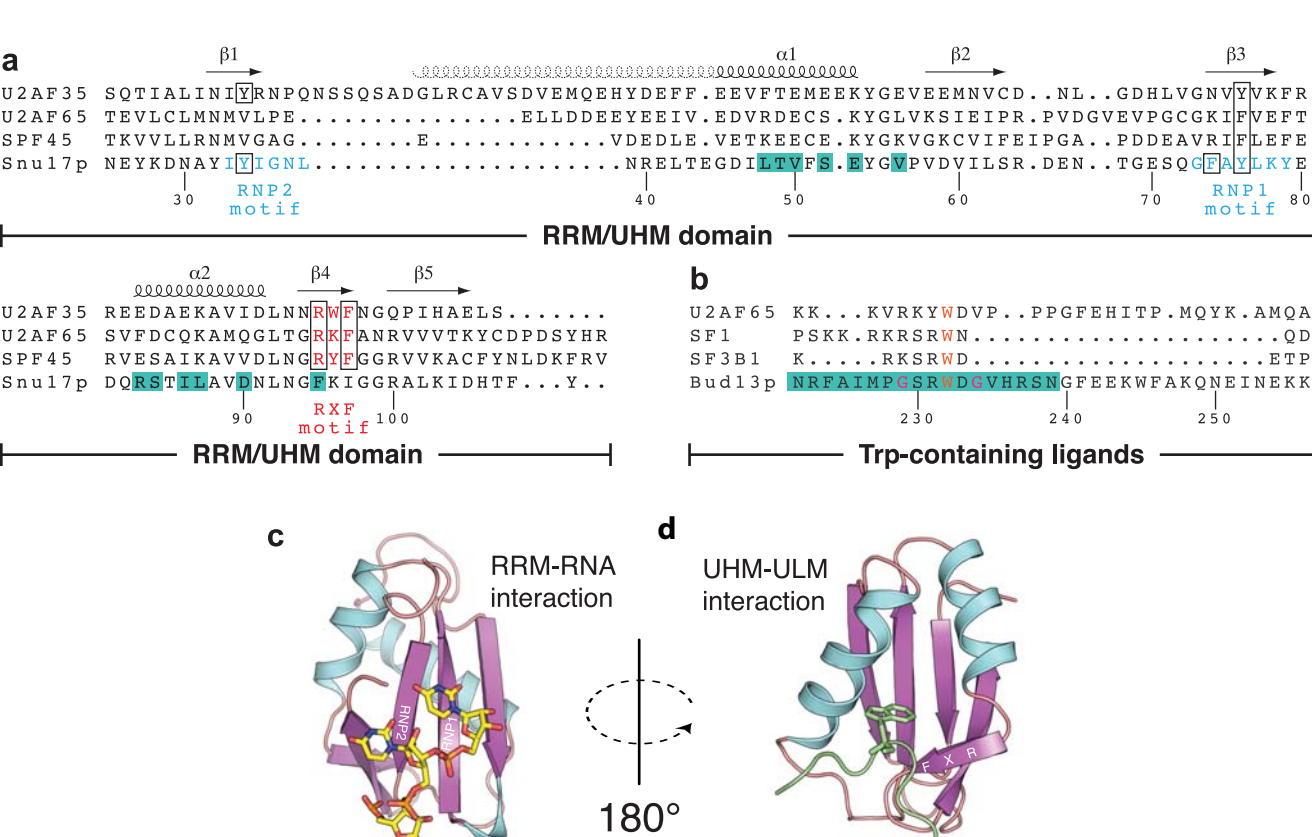
**Figure 7.** Details of the intermolecular contacts in the Snu17p-Bud13p complex. (a) The Bud13p peptide forms an arch around the helical binding surface of Snu17p. (b) Close-up views of the interaction at the entry point (left), the U-turn (middle), and the exit point (right) of the Bud13p peptide shown in (a). Interacting residues are annotated and colored blue for Snu17p and yellow for Bud13p. Intermolecular hydrogen bonds to Bud13p backbone are indicated by dashed lines.

**Figure 8.** Comparison of ligand binding modes of the UHM/RRM fold. In all panels the UHM/RRM domains are shown in the same orientation. (a) Three examples of the canonical UHM-ULM interaction. (b) PTB binding to Raver ligands which lack a Trp residue. (c) Two different binding modes of peptide partners with a Trp residue by ALYREF protein. (d) The novel Bud13p peptide recognition by Snu17p.

Table 1 NMR and refinement statistics for the Snu17p-Bud13p complex

NMR distance and dihedral restraints	
Distance restraints	
Total NOE	2607
Intra-residue	636
Inter-residue	1971
Sequential $( i-j =1)$	682
Medium-range $( i-j  < 4)$	413
Long-range $( i-j  > 5)$	747
Intermolecular	129
Total dihedral angle restraints	177
$\phi$	87
Ψ	90
Structure statistics	
Violations (mean $\pm$ s.d.)	
Distance restraints (Å)	$0.011 \pm 0.00$
Dihedral angle restraints (°)	$0.767 \pm 0.07$
Max. dihedral angle violation (°)	5.79
Max. distance restraint violation (Å)	0.34
Deviations from idealized geometry	
Bond lengths (Å)	$0.011 \pm 0.00$
Bond angles (°)	$1.206 \pm 0.03$
Impropers (°)	$1.297 \pm 0.06$
Average pairwise r.m.s. deviation** (Å)	
Heavy	$1.15 \pm 0.17$
Backbone	$0.55 \pm 0.12$
Ramachandran plot statistics (%)	
Residues in most favoured regions	93.4
Residues in additionally allowed regions	6.6

<sup>\*\*</sup> Pairwise r.m.s. deviation was calculated among 20 refined structures for residues 30-109 of Snu17p and 222-239 of Bud13p. The atomic coordinates and restraint files (code 4UQT) have been deposited in the Protein Data Bank (http://wwpdb.org/). The chemical shifts are available at the Biological Magnetic Resonance Bank (BMRB) with accession number 25047.



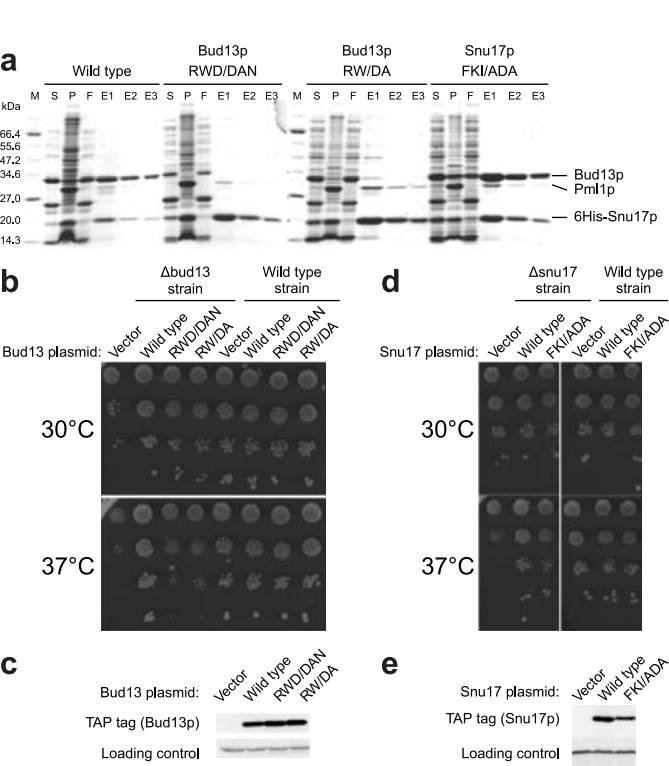
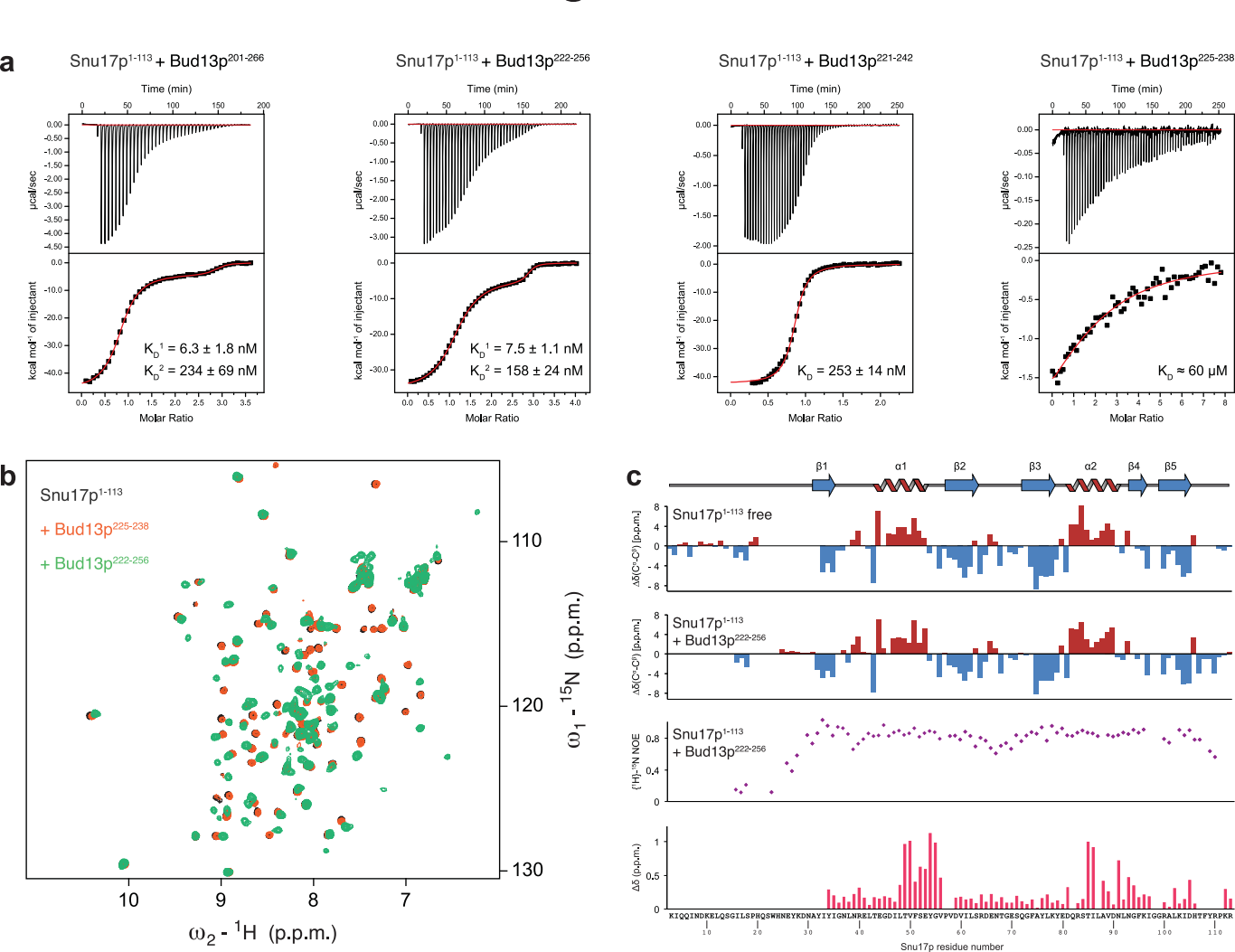
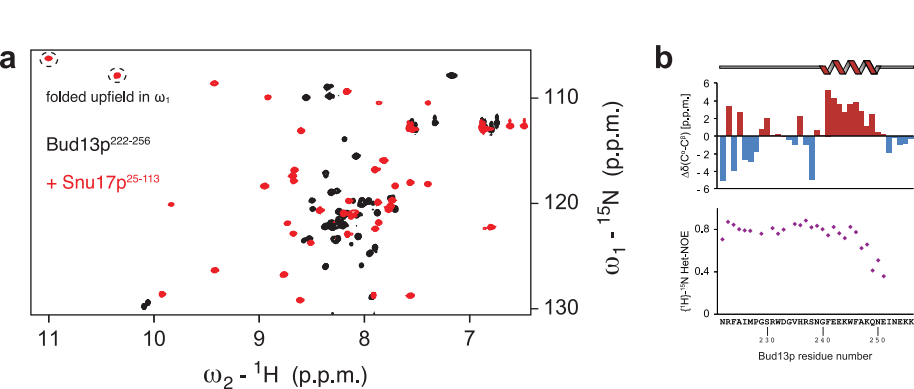


Figure 3





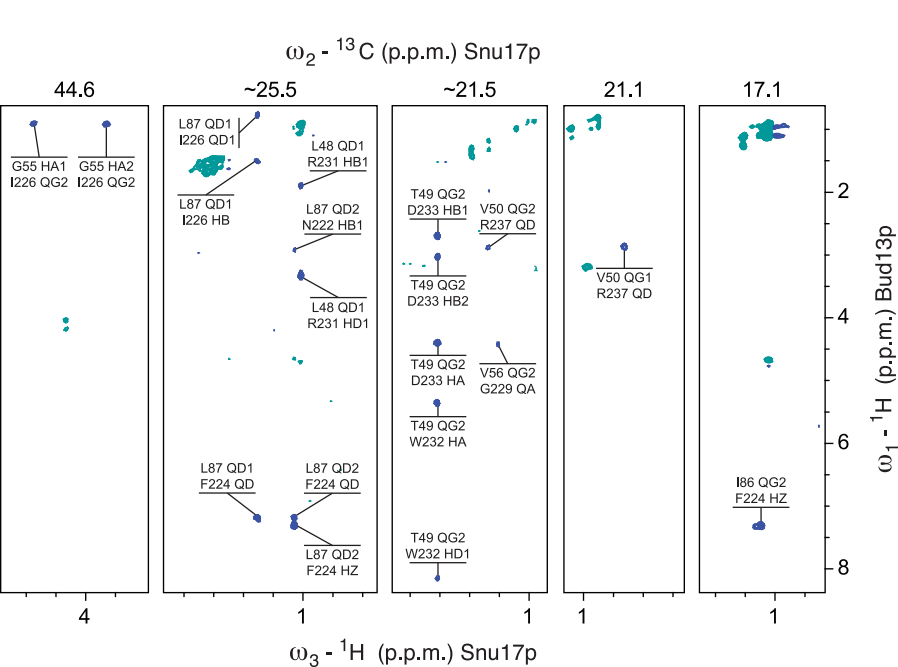


Figure 6

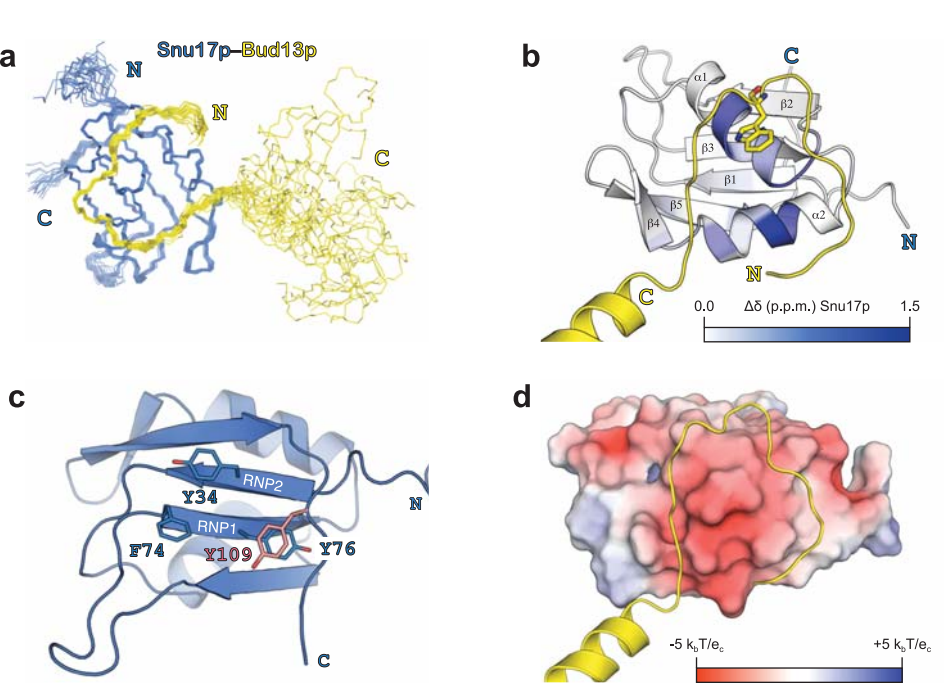
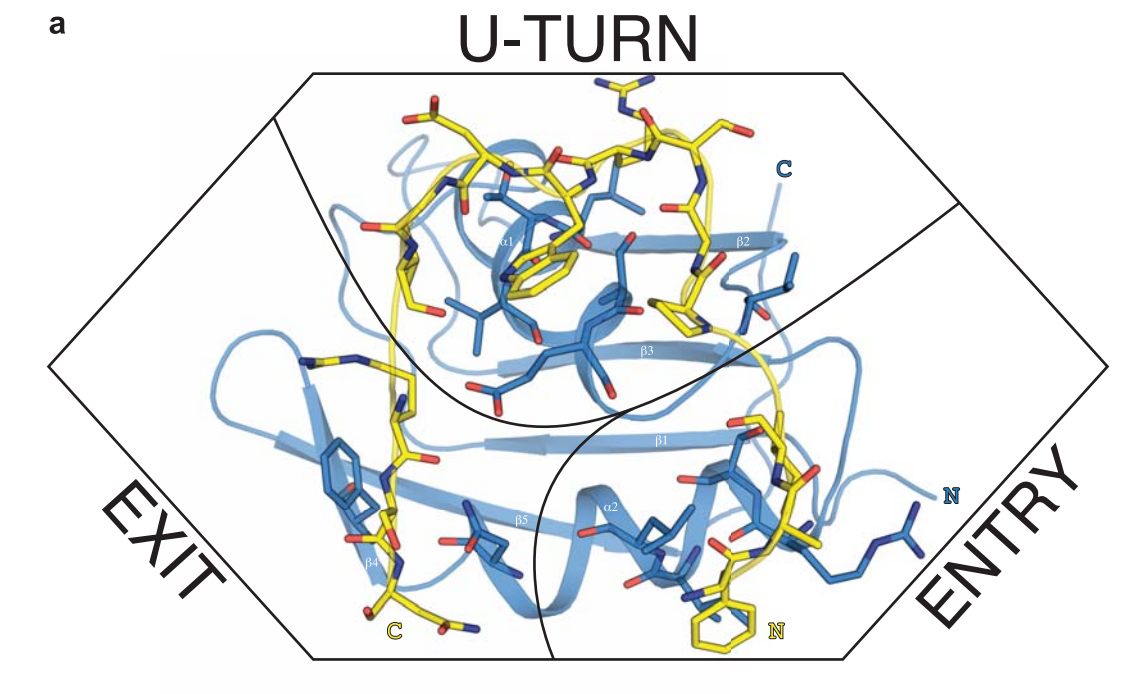
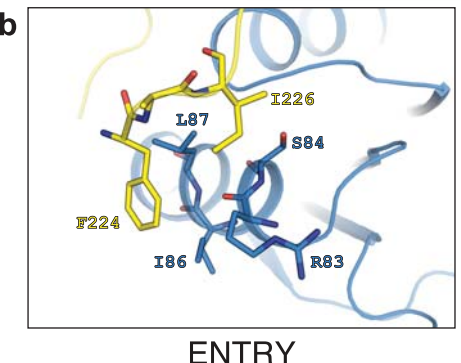
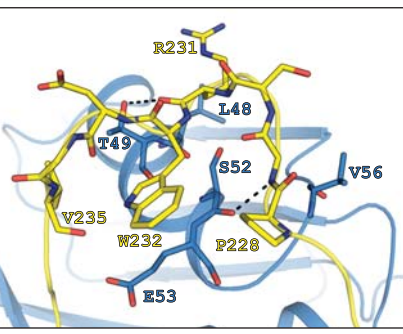


Figure 7







**U-TURN** 

